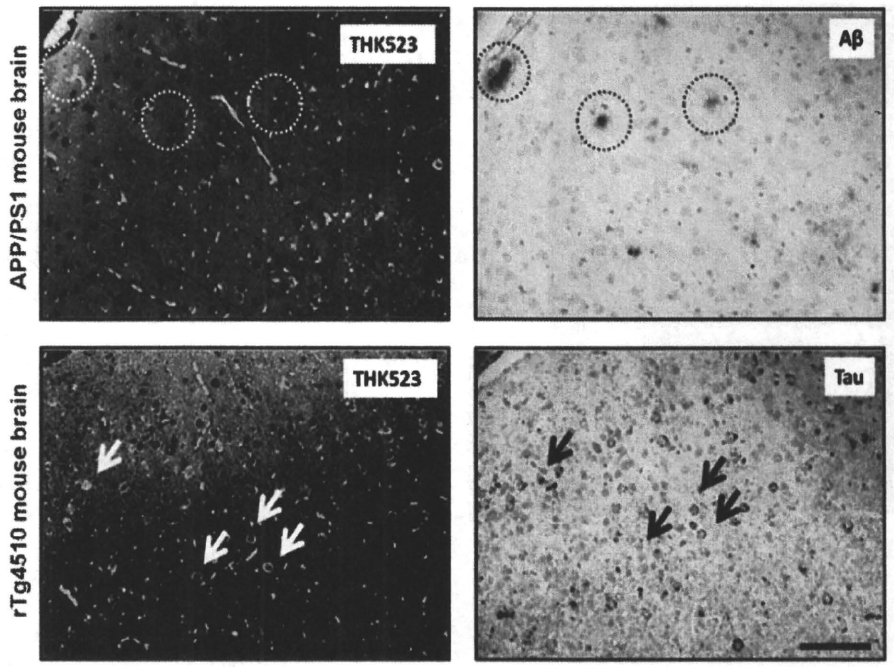

Figure 8 Co-localization of THK523 staining with tau pathology. Microscopy images of two serial sections (5 μm) from brains of rTg4510 and APP/PS1 mice immunostained with either tau (DAKO) or β-amyloid (1E8) antibodies, to identify tau tangles and β-amyloid (Aβ) plaques respectively; or stained with 10 nM THK523. Arrows indicate the location of tau tangles while circles indicate the location of β-amyloid plaques. Positive THK523 staining co-localize with tau immunostaining of neurofibrillary tangles, but not with β-amyloid plaques. Tissue sections were imaged with a Zeiss microscope and Axiocam digital camera. Scale bars: 100 μm. These data are representative of four independent studies employing eight rTg4510 and three APP/PS1 mice.

contribute differentially to the retention of ^{18}F-THK523 in the mouse brain. Similarly, as was observed in the *ex vivo* biodistribution studies, accumulation of radioactivity was observed within the intestine and liver of both rTg4510 and their control littermates indicating that most of the tracer and/or its metabolites were eliminated rapidly from the body through biliary excretion. Both tau transgenic and control littermates exhibited similar, low expression levels of tau in the liver (data not shown), further suggesting that ^{18}F-THK523 liver retention was due to the metabolic processing of ^{18}F-THK523 and not attributable to tau expression.

In conclusion, ^{18}F-THK523 is a novel tau radiotracer that fulfils the major criteria necessary for an 'ideal' PET radiotracer (Laruelle *et al.*, 2003; Nordberg, 2004). In addition to the abovementioned properties, THK523 was successfully labelled with ^{18}F with high specific activity. The relatively longer half-life of ^{18}F (110 min) precludes the need for an onsite cyclotron, allowing widespread distribution.

The clinical application of ^{18}F-THK523 as a selective tau imaging biomarker will provide important information regarding tau pathophysiology in Alzheimer's disease and non-Alzheimer's disease tauopathies, allowing correlation of brain tau load with cognitive function, monitoring disease progression and evaluation of therapeutic efficacy of newly developed drugs; especially aimed at modulating tau pathology (Gozes *et al.*, 2009; Hampel *et al.*, 2009*a*, *b*; Wischik and Staff, 2009). This study provides an important and critical step in defining the role of ^{18}F-THK523 as a tau specific PET radiotracer.

Acknowledgements

We thank Fairlie Hinton and Geoff Pavey from the Victorian Brain bank Network for sourcing and preparation of the human brain tissue.

Funding

National Health and Medical Research Council of Australia (in part); Neurosciences Victoria and the Ministry of Health, Labour and Welfare, Japan (in part); Industrial Technology Research Grant Program in 2009 from New Energy and Industrial Technology Development Organization (NEDO) of Japan(in part); AAR Viertel Fellowship (to M.T.F.-T.); NHMRC Senior Research Fellowship (to R.C. and K.J.B.). Perpetual Trustees H & L Hecht Trust.

References

Agdeppa ED, Kepe V, Liu J, Flores-Torres S, Satyamurthy N, Petric A, et al. Binding characteristics of radiofluorinated

6-dialkylamino-2-naphthylethylidene derivatives as positron emission tomography imaging probes for beta-amyloid plaques in Alzheimer's disease. J Neurosci 2001; 21: RC189.

Arriagada PV, Growdon JH, Hedley-Whyte ET, Hyman BT. Neurofibrillary tangles but not senile plaques parallel duration and severity of Alzheimer's disease. Neurology 1992; 42 (3 Pt 1): 631–9.

Barghorn S, Davies P, Mandelkow E. Tau paired helical filaments from Alzheimer's disease brain and assembled in vitro are based on beta-structure in the core domain. Biochemistry 2004; 43: 1694–703.

Blennow K, Hampel H. CSF markers for incipient Alzheimer's disease. Lancet Neurol 2003; 2: 605–13.

Cairns NJ, Ikonomovic MD, Benzinger T, Storandt M, Fagan AM, Shah A, et al. Absence of Pittsburgh compound B detection of cerebralamyloid beta in a patient with clinical, cognitive, and cerebrospinal fluidmarkers of Alzheimer disease. Arch Neurol 2009; 66: 1557–62.

Choi SR, Golding G, Zhuang Z, Zhang W, Lim N, Hefti F, et al. Preclinical properties of 18F-AV-45: a PET agent for Abeta plaques in the brain. J Nucl Med 2009; 50: 1887–94.

Delaere P, Duyckaerts C, Brion JP, Poulain V, Hauw JJ. Tau, paired helical filaments and amyloid in the neocortex: a morphometric study of 15 cases with graded intellectual status in aging and senile dementia of Alzheimer type. Acta neuropathologica 1989; 77: 645–53.

Delaere P, Duyckaerts C, Masters C, Beyreuther K, Piette F, Hauw JJ. Large amounts of neocortical beta A4 deposits without neuritic plaques nor tangles in a psychometrically assessed, non-demented person. Neurosci Lett 1990; 116: 87–93.

Dickson DW. Neuropathological diagnosis of Alzheimer's disease: a perspective from longitudinal clinicopathological studies. Neurobiology of aging 1997; 18 (Suppl 4): S21–6.

Dishino DD, Welch MJ, Kilbourn MR, Raichle ME. Relationship between lipophilicity and brain extraction of C-11-labeled radiopharmaceuticals. J Nucl Med 1983; 24: 1030–8.

Duyckaerts C, Brion JP, Hauw JJ, Flament-Durand J. Quantitative assessment of the density of neurofibrillary tangles and senile plaques in senile dementia of the Alzheimer type. Comparison of immunocytochemistry with a specific antibody and Bodian's protargol method. Acta neuropathologica 1987; 73: 167–70.

Duyckaerts C, Delaere P, Hauw JJ, Abbamondi-Pinto AL, Sorbi S, Allen I, et al. Rating of the lesions in senile dementia of the Alzheimer type: concordance between laboratories. A European multicenter study under the auspices of EURAGE. J Neurol Sci 1990; 97: 295–323.

Ferreira ST, Vieira MN, De Felice FG. Soluble protein oligomers as emerging toxins in Alzheimer's and other amyloid diseases. IUBMB Life 2007; 59: 332–45.

Fodero-Tavoletti MT, Rowe CC, McLean CA, Leone L, Li QX, Masters CL, et al. Characterization of PiB binding to white matter in Alzheimer disease and other dementias. J Nucl Med 2009; 50: 198–204.

Fodero-Tavoletti MT, Smith DP, McLean CA, Adlard PA, Barnham KJ, Foster LE, et al. In vitro characterization of Pittsburgh compound-B binding to Lewy bodies. J Neurosci 2007; 27: 10365–71.

Ganzer S, Arlt S, Schoder V, Buhmann C, Mandelkow EM, Finckh U, et al. CSF-tau, CSF-Abeta1-42, ApoE-genotype and clinical parameters in the diagnosis of Alzheimer's disease: combination of CSF-tau and MMSE yields highest sensitivity and specificity. J Neural Transm 2003; 110: 1149–60.

Gozes I, Stewart A, Morimoto B, Fox A, Sutherland K, Schmeche D. Addressing Alzheimer's disease tangles: from NAP to AL-108. Curr Alzheimer Res 2009; 6: 455–60.

Hampel H, Blennow K, Shaw LM, Hoessler YC, Zetterberg H, Trojanowski JQ. Total and phosphorylated tau protein as biological markers of Alzheimer's disease. Exp Gerontol 2009a; 45: 30–40.

Hampel H, Ewers M, Burger K, Annas P, Mortberg A, Bogstedt A, et al. Lithium trial in Alzheimer's disease: a randomized, single-blind, placebo-controlled, multicenter 10-week study. J Clin Psychiatry 2009b; 70: 922–31.

Ho GJ, Gregory EJ, Smirnova IV, Zoubine MN, Festoff BW. Cross-linking of beta-amyloid protein precursor catalyzed by tissue transglutaminase. FEBS Lett 1994; 349: 151–4.

Holcomb LA, Gordon MN, Jantzen P, Hsiao K, Duff K, Morgan D. Behavioral changes in transgenic mice expressing both amyloid precursor protein and presenilin-1 mutations: lack of association with amyloid deposits. Behav Genet 1999; 29: 177–85.

Ikonomovic MD, Klunk WE, Abrahamson EE, Mathis CA, Price JC, Tsopelas ND, et al. Post-mortem correlates of in vivo PiB-PET amyloid imaging in a typical case of Alzheimer's disease. Brain 2008; 131 (Pt 6): 1630–45.

Jack CR Jr, Knopman DS, Jagust WJ, Shaw LM, Aisen PS, Weiner MW, et al. Hypothetical model of dynamic biomarkers of the Alzheimer's pathological cascade. Lancet Neurol 2010; 9: 119–28.

Katzman R, Terry R, DeTeresa R, Brown T, Davies P, Fuld P, et al. Clinical, pathological, and neurochemical changes in dementia: a subgroup with preserved mental status and numerous neocortical plaques. Ann Neurol 1988; 23: 138–44.

Kepe V, Huang SC, Small GW, Satyamurthy N, Barrio JR. Visualizing pathology deposits in the living brain of patients with Alzheimer's disease. Methods Enzymol 2006; 412: 144–60.

Klunk WE, Engler H, Nordberg A, Wang Y, Blomqvist G, Holt DP, et al. Imaging brain amyloid in Alzheimer's disease with Pittsburgh Compound-B. Ann Neurol 2004; 55: 306–19.

Klunk WE, Lopresti BJ, Ikonomovic MD, Lefterov IM, Koldamova RP, Abrahamson EE, et al. Binding of the positron emission tomography tracer Pittsburgh compound-B reflects the amount of amyloid-beta in Alzheimer's disease brain but not in transgenic mouse brain. J Neurosci 2005; 25: 10598–606.

Lambert MP, Viola KL, Chromy BA, Chang L, Morgan TE, Yu J, et al. Vaccination with soluble Abeta oligomers generates toxicity-neutralizing antibodies. J Neurochem 2001; 79: 595–605.

Laruelle M, Slifstein M, Huang Y. Relationships between radiotracer properties and image quality in molecular imaging of the brain with positron emission tomography. Mol Imaging Biol 2003; 5: 363–75.

Lee VM, Goedert M, Trojanowski JQ. Neurodegenerative tauopathies. Annu Rev Neurosci 2001; 24: 1121–59.

LeVine H 3rd. Quantification of beta-sheet amyloid fibril structures with thioflavin T. Methods Enzymol 1999; 309: 274–84.

Maeda J, Ji B, Irie T, Tomiyama T, Maruyama M, Okauchi T, et al. Longitudinal, quantitative assessment of amyloid, neuroinflammation, and anti-amyloid treatment in a living mouse model of Alzheimer's disease enabled by positron emission tomography. J Neurosci 2007; 27: 10957–68.

Maezawa I, Hong HS, Liu R, Wu CY, Cheng RH, Kung MP, et al. Congo red and thioflavin-T analogs detect Abeta oligomers. J Neurochem 2008; 104: 457–68.

McLean CA, Cherny RA, Fraser FW, Fuller SJ, Smith MJ, Beyreuther K, et al. Soluble pool of Abeta amyloid as a determinant of severity of neurodegeneration in Alzheimer's disease. Annals Neurol 1999; 46: 860–6.

Ng S, Villemagne VL, Berlangieri S, Lee ST, Cherk M, Gong SJ, et al. Visual assessment versus quantitative assessment of 11C-PIB PET and 18F-FDG PET for detection of Alzheimer's disease. J Nucl Med 2007; 48: 547–52.

Nordberg A. PET imaging of amyloid in Alzheimer's disease. Lancet Neurol 2004; 3: 519–27.

Okamura N, Suemoto T, Furumoto S, Suzuki M, Shimadzu H, Akatsu H, et al. Quinoline and benzimidazole derivatives: candidate probes for in vivo imaging of tau pathology in Alzheimer's disease. J Neurosci 2005; 25: 10857–62.

Perez M, Valpuesta JM, Medina M, Montejo de Garcini E, Avila J. Polymerization of tau into filaments in the presence of heparin: the minimal sequence required for tau-tau interaction. J Neurochem 1996; 67: 1183–90.

Pike VW. PET radiotracers: crossing the blood-brain barrier and surviving metabolism. Trends Pharmacol Sci 2009; 30: 431–40.

Pike KE, Savage G, Villemagne VL, Ng S, Moss SA, Maruff P, et al. Beta-amyloid imaging and memory in non-demented individuals: evidence for preclinical Alzheimer's disease. Brain 2007; 130 (Pt 11): 2837–44.

Rowe CC, Ackerman U, Browne W, Mulligan R, Pike KL, O'Keefe G, et al. Imaging of amyloid beta in Alzheimer's disease with 18F-BAY94-9172, a novel PET tracer: proof of mechanism. Lancet Neurol 2008; 7: 129–35.

Rowe CC, Ng S, Ackermann U, Gong SJ, Pike K, Savage G, et al. Imaging beta-amyloid burden in aging and dementia. Neurology 2007; 68: 1718–25.

Shoghi-Jadid K, Small GW, Agdeppa ED, Kepe V, Ercoli LM, Siddarth P, et al. Localization of neurofibrillary tangles and beta-amyloid plaques in the brains of living patients with Alzheimer disease. Am J Geriatr Psychiatry 2002; 10: 24–35.

van der Zee J, Sleegers K, Van Broeckhoven C. Invited article: the Alzheimer disease-frontotemporal lobar degeneration spectrum. Neurology 2008; 71: 1191–7.

Van Dort ME, Jung YW, Sherman PS, Kilbourn MR, Wieland DM. Fluorine for hydroxy substitution in biogenic amines: asymmetric synthesis and biological evaluation of fluorine-18-labeled beta-fluorophenylalkylamines as model systems. J Med Chem 1995; 38: 810–5.

von Bergen M, Barghorn S, Jeganathan S, Mandelkow EM, Mandelkow E. Spectroscopic approaches to the conformation of tau protein in solution and in paired helical filaments. Neurodegener Dis 2006; 3: 197–206.

Walsh DM, Klyubin I, Fadeeva JV, Cullen WK, Anwyl R, Wolfe MS, et al. Naturally secreted oligomers of amyloid beta protein potently inhibit hippocampal long-term potentiation in vivo. Nature 2002; 416: 535–9.

Wenk GL. Neuropathologic changes in Alzheimer's disease. J Clin Psychiatry 2003; 64 (Suppl 9): 7–10.

Wischik C, Staff R. Challenges in the conduct of disease-modifying trials in Alzheimer's disease: practical experience from a phase 2 trial of Tau-aggregation inhibitor therapy. J Nutr Health Aging 2009; 13: 367–9.

Wisniewski HM, Bancher C, Barcikowska M, Wen GY, Currie J. Spectrum of morphological appearance of amyloid deposits in Alzheimer's disease. Acta Neuropathol 1989; 78: 337–47.

doi:10.1093/brain/awq091 Brain 2010: 133; 1772–1778 | 1772

BRAIN
A JOURNAL OF NEUROLOGY

In vivo visualization of α-synuclein deposition by carbon-11-labelled 2-[2-(2-dimethylaminothiazol-5-yl)ethenyl]-6-[2-(fluoro)ethoxy]benzoxazole positron emission tomography in multiple system atrophy

Akio Kikuchi,[1] Atsushi Takeda,[1] Nobuyuki Okamura,[2] Manabu Tashiro,[3] Takafumi Hasegawa,[1] Shozo Furumoto,[2,4] Michiko Kobayashi,[1] Naoto Sugeno,[1] Toru Baba,[1] Yasuo Miki,[5] Fumiaki Mori,[5] Koichi Wakabayashi,[5] Yoshihito Funaki,[4] Ren Iwata,[4] Shoki Takahashi,[6] Hiroshi Fukuda,[7] Hiroyuki Arai,[8] Yukitsuka Kudo,[9] Kazuhiko Yanai[2] and Yasuto Itoyama[1]

1 Department of Neurology, Graduate School of Medicine, Tohoku University, Sendai, 980-8574 Japan
2 Department of Pharmacology, Graduate School of Medicine, Tohoku University, Sendai, 980-8575 Japan
3 Division of Cyclotron Nuclear Medicine, Cyclotron and Radioisotope Centre, Tohoku University, Sendai, 980-8578 Japan
4 Division of Radiopharmaceutical Chemistry, Cyclotron and Radioisotope Centre, Tohoku University, Sendai, 980-8578 Japan
5 Department of Neuropathology, Institute of Brain Science, Hirosaki University Graduate School of Medicine, Hirosaki, 036-8562 Japan
6 Department of Diagnostic Radiology, Graduate School of Medicine, Tohoku University, Sendai, 980-8575 Japan
7 Department of Nuclear Medicine and Radiology, Institute of Development, Ageing and Cancer, Tohoku University, Sendai, 980-8575 Japan
8 Department of Geriatric and Respiratory Medicine, Institute of Development, Ageing and Cancer, Tohoku University, Sendai, 980-8575 Japan
9 Innovation of New Biomedical Engineering Centre, Tohoku University, Sendai, 980-8574 Japan

Correspondence to: Atsushi Takeda,
Department of Neurology,
Graduate School of Medicine,
Tohoku University,
1-1 Seiryo-machi,
Aoba-ku, Sendai, Miyagi,
980-8574, Japan
E-mail: atakeda@em.neurol.med.tohoku.ac.jp

The histopathological hallmark of multiple system atrophy is the appearance of intracellular inclusion bodies, named glial cytoplasmic inclusions, which are mainly composed of α-synuclein fibrils. *In vivo* visualization of α-synuclein deposition should be used for the diagnosis and assessment of therapy and severity of pathological progression in multiple system atrophy. Because 2-[2-(2-dimethylaminothiazol-5-yl)ethenyl]-6-[2-(fluoro)ethoxy] benzoxazole could stain α-synuclein-containing glial cytoplasmic inclusions in post-mortem brains, we compared the carbon-11-labelled 2-[2-(2-dimethylaminothiazol-5-yl)ethenyl]-6-[2-(fluoro)ethoxy] benzoxazole positron emission tomography findings of eight multiple system atrophy cases to those of age-matched normal controls. The positron emission tomography data demonstrated high distribution volumes in the subcortical white matter (uncorrected $P<0.001$), putamen and posterior cingulate cortex (uncorrected $P<0.005$), globus pallidus, primary motor cortex and anterior cingulate cortex (uncorrected $P<0.01$), and substantia nigra (uncorrected $P<0.05$) in multiple system atrophy cases compared to the normal controls. They were coincident with glial cytoplasmic inclusion-rich brain areas in

Received January 13, 2010. Revised March 15, 2010. Accepted March 17, 2010. Advance Access publication April 29, 2010

multiple system atrophy and thus, carbon-11-labelled 2-[2-(2-dimethylaminothiazol-5-yl)ethenyl]-6-[2-(fluoro)ethoxy] benzoxazole positron emission tomography is a promising surrogate marker for monitoring intracellular α-synuclein deposition in living brains.

Keywords: glial cytoplasmic inclusion; Lewy body; β-amyloid; Parkinson's disease; Pittsburgh compound B

Abbreviations: BF-227 = 2-[2-(2-dimethylaminothiazol-5-yl)ethenyl]-6-[2-(fluoro)ethoxy]benzoxazole; MSA = multiple system atrophy; PIB = Pittsburgh compound B

Introduction

Multiple system atrophy (MSA) is a sporadic, progressive neurodegenerative disease characterized by variable severity of parkinsonism, cerebellar ataxia, autonomic failure and pyramidal signs. Although MSA was originally described as three separate diseases [olivopontocerebellar atrophy (Dejerine and Thomas, 1900), striatonigral degeneration (van der Eecken *et al.*, 1960) and Shy–Drager syndrome (Shy and Drager, 1960)], they are currently classified into a single disease that consists of MSA with predominant parkinsonism and MSA with predominant cerebellar ataxia (Gilman *et al.*, 1999). The histopathological hallmark of MSA, glial cytoplasmic inclusions, comprises mainly insoluble fibrils of phosphorylated α-synuclein (Wakabayashi *et al.*, 1998). Thus, it is suggested that the MSA is in the family of α-synucleinopathies (Marti *et al.*, 2003) including Parkinson's disease and dementia with Lewy bodies, which are characterized by the presence of Lewy bodies, representing other brain inclusions composed of α-synuclein.

Previous neuropathological studies indicated that the appearance of glial cytoplasmic inclusions preceded the clinical onset of MSA (Fujishiro *et al.*, 2008) and the amount of α-synuclein deposition correlated with the disease progression (Wakabayashi and Takahashi, 2006). Therefore, it is plausible that the formation of α-synuclein deposits plays a key role in neurodegeneration, and that compounds that inhibit this process may be therapeutically useful for MSA and other α-synucleinopathies. In fact some compounds, including antioxidants (Ono and Yamada, 2006) and non-steroidal anti-inflammatory drugs (Hirohata *et al.*, 2008), were reported to have potent anti-fibrillogenic and fibril-destabilizing effects on aggregated α-synucleins, and received much attention as possible new therapeutic agents (Ono and Yamada, 2006; Hirohata *et al.*, 2008). Detection of α-synuclein deposition *in vivo* could theoretically allow early diagnosis even at the presymptomatic stage, as well as assess disease progression and possible therapeutic effects in the living brain of patients with MSA.

Although Pittsburgh compound B (PIB) and other compounds were reported to be useful in detecting senile plaques *in vivo*, to our knowledge, there were no imaging probes currently available for *in vivo* detection of α-synuclein deposition. Recently, 2-[2-(2-dimethylaminothiazol-5-yl)ethenyl]-6-[2-(fluoro)ethoxy] benzoxazole (BF-227), known as a positron emission tomography (PET) probe for *in vivo* detection of dense β-amyloid deposits in humans (Kudo *et al.*, 2007), was reported to bind with synthetic α-synuclein aggregates as well as β-amyloid fibrils *in vitro* (Fodero-Tavoletti *et al.*, 2009). In the present study, we demonstrated that BF-227 could stain α-synuclein-containing glial cytoplasmic inclusions in post-mortem tissues and moreover, that a PET study with carbon-11-labelled BF-227 ([11C]-BF-227) could detect α-synuclein deposits in the living brains of patients with MSA.

Materials and methods

Neuropathological staining

Brain specimens

The subjects of the first part of the study were nine autopsy cases, including three with Parkinson's disease, three with dementia with Lewy bodies and three with MSA. The above diagnoses were confirmed both clinically and histopathologically. Brain tissues taken from the temporal cortex and substantia nigra of patients with Parkinson's disease and dementia with Lewy bodies, and pontine base of patients with MSA, were fixed in 20% buffered formalin for 72 h at 4°C, and vibratome sections (50 μm thick) were prepared.

Fluorescence and immunohistochemical analysis

BF-227 was dissolved in 50% ethanol containing 5% polysorbate (Tween 80; Wako, Osaka, Japan). The sections were slide mounted, incubated in 100 μM BF-227 for 30 min, dipped three times in phosphate buffer, and coverslipped with non-fluorescent mounting medium (Vectashield, Vector Laboratories, Burlingame, CA, USA). Fluorescence images were visualized using an Olympus Provis fluorescence microscope (Olympus, Tokyo, Japan) at wavelength 400 nm. After photographing fluorescent structures, BF-227-labelled sections were immunostained with primary antibodies against phosphorylated α-synuclein (#64; Wako). For phosphorylated α-synuclein immunohistochemistry, the sections were pre-treated with 99% formic acid for 5 min, then incubated overnight at 4°C with each primary antibody followed by incubation with the biotinylated secondary antibodies and the avidin–biotin–peroxidase complex (Vectastain ABC kit, Vector Laboratories). Diaminobenzidine was used as the chromogen.

PET study

Subjects

Eight patients with probable MSA and eight age-matched normal subjects were studied to examine the distribution of [11C]-BF-227 in the brain. All probable MSA patients were diagnosed on the second consensus criteria for probable MSA (Gilman *et al.*, 2008). Table 1 summarizes the clinical features of these patients. There were no significant differences in age, disease duration and unified MSA rating scale score between the MSA with predominant parkinsonism

Table 1 Subject profile

	Normal controls	MSA		
		Total	MSA-P	MSA-C
n	8	8	4	4
Gender (F/M)	4/4	4/4	1/3	3/1
Age (years)	64.3 ± 5.90	57.4 ± 10.1	60.5 ± 11.1	54.3 ± 9.50
Duration (years)		1.50 ± 0.54	1.75 ± 0.50	1.25 ± 0.50
UMSARS score		36.1 ± 8.87	41.5 ± 9.39	30.8 ± 4.27

Data are mean ± SD.
MSA-P = MSA with predominant parkinsonism; MSA-C = MSA with predominant cerebellar ataxia; UMSARS = unified MSA rating scale.

subgroup and the MSA with predominant cerebellar ataxia subgroup. The normal control group comprised volunteers without impairment of cognitive and motor functions who had no cerebrovascular lesions on magnetic resonance imaging. The study protocol was approved by the Ethical Committee of Tohoku University Graduate School of Medicine, and a written informed consent was obtained from each subject after being given a complete description of the study.

Radiosynthesis of [^{11}C]-BF-227

BF-227 and its N-desmethylated derivative (a precursor of [^{11}C]-BF-227) were custom-synthesized by Tanabe R&D Service Co. (Tokyo) (Kudo *et al.*, 2007). [^{11}C]-BF-227 was synthesized from the precursor by N-methylation in dimethyl sulphoxide using [^{11}C]-methyl triflate (Jewett, 1992; Iwata *et al.*, 2001). After quenching the reaction with 5% acetic acid in ethanol, [^{11}C]-BF-227 was separated from the crude mixture by semi-preparative reversed-phase high-performance liquid chromatography and then isolated from the collected fraction by solid-phase extraction. The purified [^{11}C]-BF-227 was solubilized in isotonic saline containing 1% polysobate-80 and 5% ascorbic acid. The saline solution was filter sterilized with a 0.22 mm Millipore® filter for clinical use. The radiochemical yields were >50% based on [^{11}C]-methyl triflate, and the specific radioactivities were 119–138 GBq/mmol at the end of synthesis. The radiochemical purities were >95%.

PET procedure

The [^{11}C]-BF-227 PET study was performed using a SET-2400W PET scanner (Shimadzu Inc., Japan) under resting condition with eyes closed in a dark room. Following a 68Ge/Ga transmission scan of 300–400 s duration, an emission scan was started soon after intravenous injection of 3.7–8.3 mCi of [^{11}C]-BF-227. A dynamic series of PET scans were acquired over 60 min with 23 frames. Emission data were corrected for attenuation, dead time and radioactive decay. Standardized uptake value images were obtained by normalizing tissue concentration by the injected dose and body mass. Arterial blood samples (1.5 ml) from the radial or brachial artery were collected from each subject at 10 s intervals for the first 2 min, and subsequently at intervals increasing progressively from 1 to 10 min until 60 min after the injection of [^{11}C]-BF-227 except for one subject, from whom arterialized venous blood samples (1.5 ml) from a hand vein heated in a far-infrared mat were collected at the same time intervals. The plasma obtained by centrifugation at 3000*g* for 3 min was weighed and the radioactivity was measured with a well-type scintillation counter. Additional arterial blood samples were obtained at four time points during the study (5, 15, 30 and 60 min) for the determination of radiolabelled metabolites in plasma using high-performance liquid chromatography. These data yielded values of the unchanged fraction of parent radiotracer throughout the time frame of the study. A multi-exponential equation was used to describe this curve and to estimate the parent fraction at each measured plasma curve time point.

PET image analysis

To measure α-synuclein deposition densities in the brain, the distribution volume, the ratio of [^{11}C]-BF-227 concentration in tissue to that in plasma at equilibrium, was calculated by Logan's graphical analysis (Logan, 2000), since BF-227 reversibly binds to α-synuclein depositions (Tashiro *et al.*, 2009). Region of interest analysis was performed to evaluate the regional distribution of [^{11}C]-BF-227. Circular regions of interest were placed on individual axial PET images in the frontal cortex, primary motor cortex, parietal cortex, medial temporal cortex, lateral temporal cortex, occipital cortex, anterior cingulate cortex, posterior cingulate cortex, subcortical white matter, caudate nucleus, putamen, globus pallidus, thalamus, substantia nigra, midbrain tegmentum, pons and cerebellar cortex, referring to the individual magnetic resonance images.

Statistical analysis

Data were expressed as mean ± SD. Differences in distribution volume between normal control and MSA groups were evaluated by one-way analysis of variance followed by Bonferroni's multiple comparison test (GraphPad Prism Software).

Results

Neuropathological staining

In the post-mortem brains with Parkinson's disease, double-labelling immunostaining with BF-227 fluorostaining and anti-phosphorylated α-synuclein antibody demonstrated co-localization of the proteins in Lewy bodies in the substantia nigra (Fig. 1A and B). Strong BF-227 staining was observed in the central core (Fig. 1A). BF-227 was also detected in the cortical Lewy bodies in dementia with Lewy bodies (Fig. 1C and D). In MSA, double-labelling experiments using BF-227 and anti-phosphorylated α-synuclein antibody demonstrated BF-227 fluorescent signal in the most of glial cytoplasmic inclusions in the pontine base (Fig. 1E and F).

PET study

Tissue time activity curves of [^{11}C]-BF-227 in the brain indicated more gradual clearance from the brain in patients with MSA compared with normal subjects following initial rapid uptake of radioactivity (Fig. 2A). Relatively high concentrations of [^{11}C]-BF-227 radioactivity were observed in the subcortical white matter and lenticular nucleus in MSA, in which relatively intense α-synuclein deposits were found in the post-mortem brain (Fig. 2B). [^{11}C]-BF-227 exhibited linear regression curves on Logan plot analysis in all brain regions examined. Since the slopes of the regression lines represent the distribution volume of the tracer, these findings indicated a higher distribution volume of [^{11}C]-BF-227 in MSA than in normal controls (Fig. 2C). The regional distribution volume values were high in the subcortical white matter (uncorrected $P<0.001$), putamen and posterior cingulate cortex

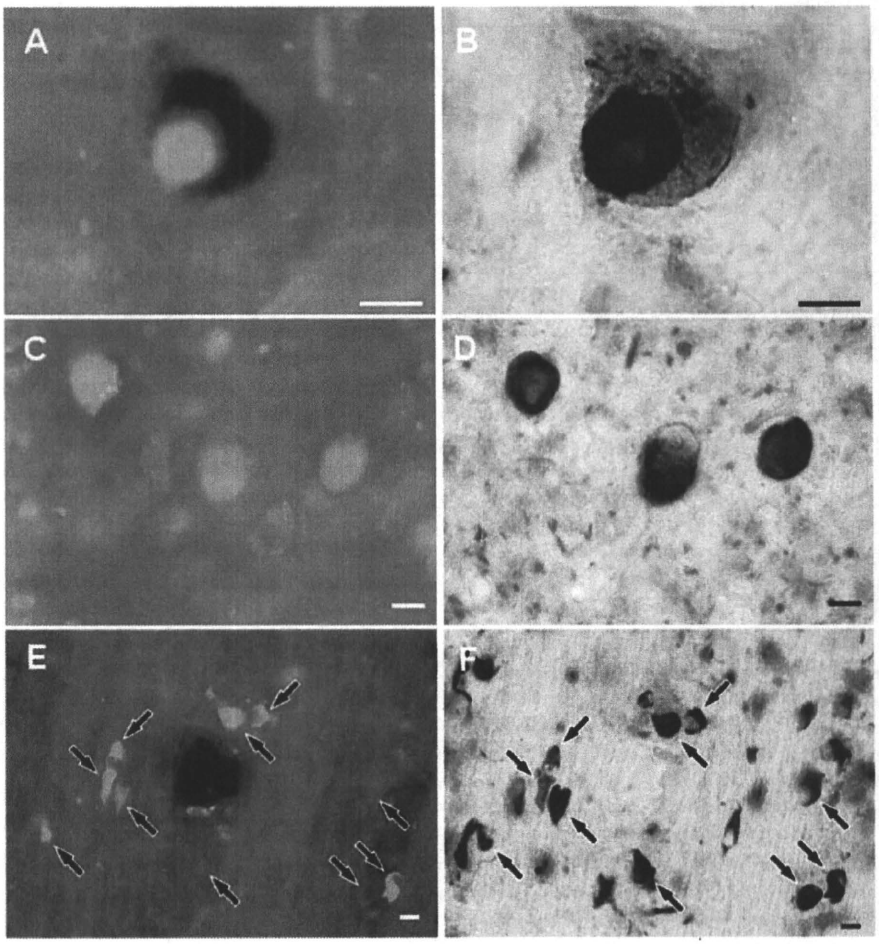

Figure 1 Neuropathological findings of BF-227 fluorostaining and anti-phosphorylated α-synuclein antibody immunostaining. BF-227 fluorostaining (**A** and **C**) and anti-phosphorylated α-synuclein antibody immunostaining (**B** and **D**) showed colocalization of these proteins in brainstem-type Lewy bodies in the substantia nigra of patients with Parkinson's disease (**A** and **B**) and in cortical Lewy bodies in the temporal lobe of patients dementia with Lewy bodies (**C** and **D**). Similarly, BF-227 fluorostaining (**E**) and anti-phosphorylated α-synuclein antibody immunostaining (**F**) were codetected in glial cytoplasmic inclusions in the pontine base of a patient with MSA. BF-227 histofluorescence was observed in the most of glial cytoplasmic inclusions (arrows). Bars = 10 μm.

(uncorrected $P<0.005$), globus pallidus, primary motor cortex and anterior cingulate cortex (uncorrected $P<0.01$) and substantia nigra (uncorrected $P<0.05$) in patients with MSA compared to the normal controls (Table 2 and Fig. 2D). It is noteworthy that the distribution volume of [11C]-BF-227 was significantly high in the subcortical white matter even if Bonferroni's multiple comparison test was applied. On the other hand, no obvious differences were found in either the distribution or degree of binding between the MSA with predominant parkinsonism and MSA with predominant cerebellar ataxia subgroups.

Discussion

The BF-227 stained α-synuclein-containing Lewy bodies (Fig. 1A–D) and glial cytoplasmic inclusions (Fig. 1E and F) in formalin-fixed tissue sections as well as β-amyloid-containing senile plaques in paraffin-embedded tissue sections (Kudo *et al.*, 2007). These results were consistent with the previous findings showing BF-227 binding to synthetic α-synuclein fibrils with high affinity (K_d 9.63 nM) (Fodero-Tavoletti *et al.*, 2009), and to Lewy bodies in paraffin-embedded tissue sections (Fodero-Tavoletti *et al.*, 2009).

The anti-phosphorylated α-synuclein antibody immunostained the halo region more intensively compared with the central core in Lewy bodies in the substantia nigra of Parkinson's disease, while the BF-227 staining was intensely observed in the core of Lewy bodies (Fig. 1A and B). Because intense thioflavin S staining was also reported in the core of nigral Lewy bodies (Duda *et al.*, 2000), the core is thought to be rich in β-sheet structures. Similar to thioflavin S, the BF-227 staining is considered to recognize amyloid-like β-pleated sheets, and it was suggested to be the reason for the more intense BF-227 staining in the core of Lewy bodies. In addition, the high density of the core structure

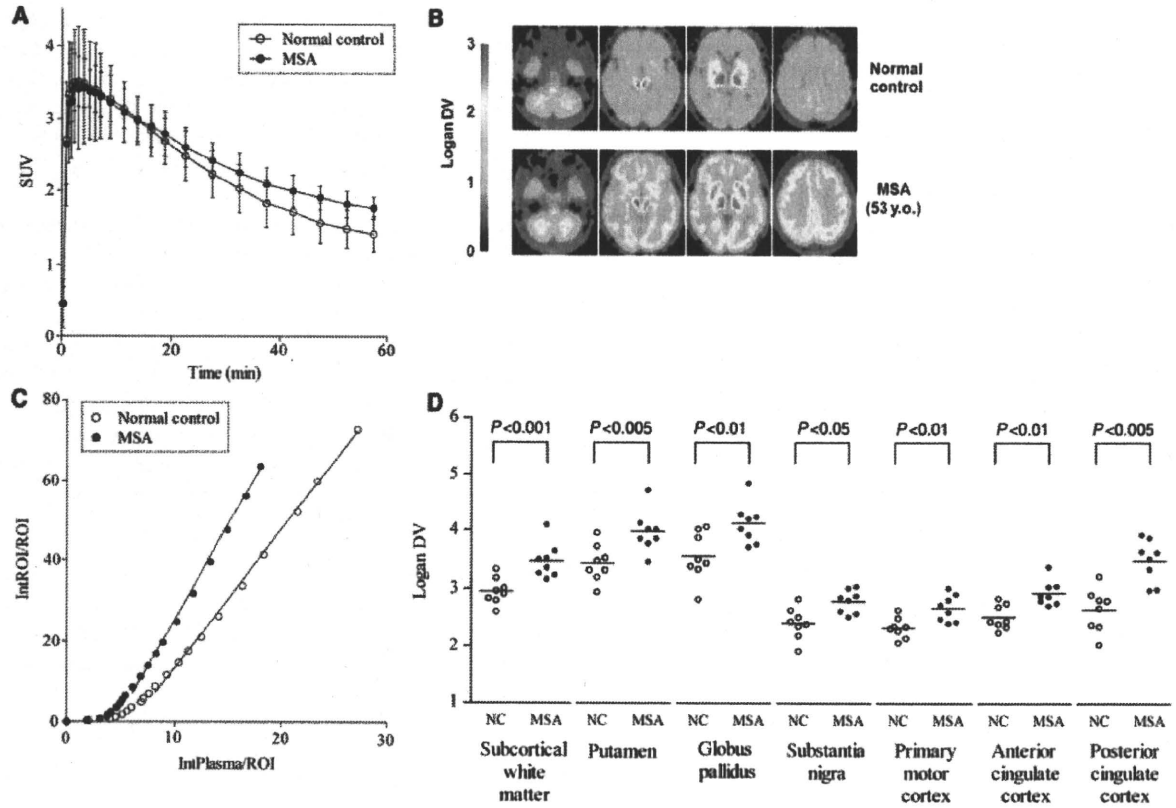

Figure 2 [^{11}C]-BF-227 PET findings in MSA. Time activity curves showed initial rapid uptake of radioactivity followed by gradual clearance in the putamen of both normal subjects and MSA cases. Data are mean ± SD of eight normal subjects and eight patients with MSA (**A**). In a representative patient with MSA with predominant cerebellar ataxia, the regional distribution volumes were mapped to the subcortical white matter and lentiform nucleus compared to normal control (**B**). Typical Logan plots for the putamen were presented in a representative patient with MSA with predominant cerebellar ataxia and a normal control. The slopes of the linear regression curves on Logan plot analysis represent the distribution volume of the tracer in the putamen (**C**). There were differences in the mean regional distribution volume values between patients with MSA and normal control in the subcortical white matter (uncorrected $P<0.001$), putamen and posterior cingulate cortex (uncorrected $P<0.005$), globus pallidus, primary motor cortex and anterior cingulate cortex (uncorrected $P<0.01$) and substantia nigra (uncorrected $P<0.05$). Data of individual subjects (symbols) and mean values (horizontal lines) (**D**). SUV = standardized uptake value; DV = distribution volume; ROI = region of interest.

may often prevent the penetration of antibodies into this region (Galloway *et al.*, 1992), since electron microscopic studies revealed that vesicular structures were tightly packed in the core of Lewy bodies (Takahashi and Wakabayashi, 2005). On the other hand, not all glial cytoplasmic inclusions stained by anti-phosphorylated α-synuclein antibody were always positive for BF-227 staining (Fig. 1E and F). In the process of oligodendroglial pathology, it was believed that α-synuclein deposits as amorphous state and then forms fibrillar structures (Gai *et al.*, 2003; Stefanova *et al.*, 2005). In fact, part of glial cytoplasmic inclusions were reported to be α-synuclein-negative (Sakamoto *et al.*, 2005) and therefore, it seems reasonable that some of glial cytoplasmic inclusions were not composed of β-sheet fibrils and were negative for BF-227 staining.

The regional distribution volume of [^{11}C]-BF-227 was the highest in the subcortical white matter, followed by the putamen, posterior cingulate cortex, anterior cingulate cortex, globus pallidus, primary motor cortex and substantia nigra, in which glial cytoplasmic inclusions were densely distributed (Papp and Lantos, 1994; Inoue *et al.*, 1997; Wakabayashi and Takahashi, 2006) and large increases of α-synuclein content were found (Tong *et al.*, 2010) in the post-mortem brains. Thus, it was suggested that the distributions of [^{11}C]-BF-227 could properly reflect those of the α-synuclein deposits *in vivo*. On the other hand, the regional distribution volume in other affected brain regions, such as the cerebellum and pons (Ozawa *et al.*, 2004; Wakabayashi and Takahashi, 2006), did not show higher values relative to the normal control group. The glial cytoplasmic inclusions in cerebellum were reported to decrease along with the disease progression and concomitant neuronal loss (Inoue *et al.*, 1997). Therefore, it is plausible that the accumulation levels of glial cytoplasmic inclusions are changing and do not always increase with the disease progression (Mochizuki *et al.*, 1992; Inoue *et al.*, 1997). Moreover, due to the remarkable cerebellar and pontine atrophy,

Table 2 **Distribution volume of [^{11}C]BF-227**

	Normal controls	MSA
Frontal cortex	2.28 ± 0.18	2.46 ± 0.22
Primary motor cortex	2.40 ± 0.28	2.79 ± 0.20¶
Parietal cortex	2.48 ± 0.26	2.63 ± 0.24
Medial temporal cortex	2.44 ± 0.21	2.82 ± 0.31
Lateral temporal cortex	2.42 ± 0.19	2.63 ± 0.23
Occipital cortex	2.43 ± 0.20	2.72 ± 0.27
Anterior cingulate cortex	2.32 ± 0.18	2.67 ± 0.23¶
Posterior cingulate cortex	2.52 ± 0.22	2.94 ± 0.22†
Subcortical white matter	2.65 ± 0.38	3.49 ± 0.36‡
Caudate nucleus	2.70 ± 0.21	3.05 ± 0.34
Putamen	2.95 ± 0.23	3.47 ± 0.30†
Globus pallidus	3.43 ± 0.31	3.97 ± 0.36¶
Thalamus	3.50 ± 0.28	4.03 ± 0.31
Substantia nigra	3.55 ± 0.41	4.12 ± 0.36*
Midbrain tegmentum	3.53 ± 0.54	3.45 ± 0.47
Pons	3.63 ± 0.54	3.88 ± 0.42
Cerebellar cortex	2.32 ± 0.22	2.16 ± 0.29

Data are mean ± SD.
*Uncorrected $P < 0.05$.
¶Uncorrected $P < 0.01$.
†Uncorrected $P < 0.005$.
‡Uncorrected $P < 0.001$.

the distribution volume in these regions might be underestimated. Correction for partial volume loss is therefore needed to improve the accuracy of quantification in the cerebellum and brainstem of MSA. BF-227 fluorescent signal was detected in β-amyloid plaques as well as glial cytoplasmic inclusions and Lewy bodies (Fig. 1A–F) in neuropathological staining (Kudo *et al.*, 2007). However, the differences in the distribution of [^{11}C]-BF-227 by PET could discriminate MSA from Alzheimer's disease, which showed high distribution of [^{11}C]-BF-227 in the temporoparietal–occipital region (Kudo *et al.*, 2007). In our preliminary studies, Parkinson's disease and dementia with Lewy bodies also showed quite different patterns of distribution volumes from those of MSA (data not shown). Therefore, MSA could be distinguished from other degenerative diseases such as Alzheimer's disease, Parkinson's disease and dementia with Lewy bodies by the [^{11}C]-BF-227 PET.

The affinity of BF-227 to α-synuclein fibrils (K_d 9.63 nM) was reported to be almost identical to that of PIB (K_d 10.07 nM) (Fodero-Tavoletti *et al.*, 2007, 2009). However, in the post-mortem human brain, the PIB binding was not colocalized with α-synuclein-positive Lewy bodies in two reports (Fodero-Tavoletti *et al.*, 2007; Ye *et al.*, 2008) although one report showed PIB binding to Lewy bodies in the substantia nigra of Parkinson's disease (Maetzler *et al.*, 2008). Therefore, there is controversy as to whether PIB binds to α-synuclein-containing Lewy bodies. Moreover, there have been no reports showing that PIB could detect α-synuclein deposits in α-synucleinopathies by PET (Fodero-Tavoletti *et al.*, 2007; Johansson *et al.*, 2008; Maetzler *et al.*, 2008). The hydroxy group in PIB (Mathis *et al.*, 2003) may prevent it from passing through the cell membranes and thereby detecting α-synuclein depositions in the cytoplasm, however, the BF-227 is more lipophilic than PIB (Mathis *et al.*, 2003), and may easily pass into the cytoplasm and bind to α-synuclein aggregates. As shown in the present study, BF-227 is a promising tracer to detect glial cytoplasmic inclusions. Further studies are warranted to verify whether Lewy bodies in other α-synucleinopathies as well as glial cytoplasmic inclusions can be detected by [^{11}C]-BF-227 PET.

In conclusion, the BF-227 could bind to α-synuclein-containing glial cytoplasmic inclusions (Fig. 1E and F) in the post-mortem brain, and the [^{11}C]-BF-227 PET demonstrated high signals in the glial cytoplasmic inclusion-rich brain regions including subcortical white matter, putamen, globus pallidus, primary motor cortex and anterior and posterior cingulate cortex (Table 2 and Fig. 2D). These results suggest that [^{11}C]-BF-227 PET is a suitable surrogate maker for monitoring α-synuclein deposits in living brains with MSA and could be a potential tool to monitor the effectiveness of neuroprotective therapy for α-synucleinopathies.

Funding

Grant for 'the Research Committee for Ataxic Diseases' of the Research on Measures for Intractable Diseases from the Ministry of Health, Labour and Welfare, Japan (partial).

References

Dejerine J, Thomas A. L'atrophie olivo-ponto-cérébelleuse. Nouvelle Iconographie Salpêtrière 1900; 13: 330–7.

Duda JE, Lee VM, Trojanowski JQ. Neuropathology of synuclein aggregates. J Neurosci Res 2000; 61: 121–7.

Fodero-Tavoletti MT, Mulligan RS, Okamura N, Furumoto S, Rowe CC, Kudo Y, et al. In vitro characterisation of BF227 binding to alpha-synuclein/Lewy bodies. Eur J Pharmacol 2009; 617: 54–8.

Fodero-Tavoletti MT, Smith DP, McLean CA, Adlard PA, Barnham KJ, Foster LE, et al. In vitro characterization of Pittsburgh compound-B binding to Lewy bodies. J Neurosci 2007; 27: 10365–71.

Fujishiro H, Ahn TB, Frigerio R, DelleDonne A, Josephs KA, Parisi JE, et al. Glial cytoplasmic inclusions in neurologically normal elderly: prodromal multiple system atrophy? Acta Neuropathol 2008; 116: 269–75.

Gai WP, Pountney DL, Power JH, Li QX, Culvenor JG, McLean CA, et al. alpha-Synuclein fibrils constitute the central core of oligodendroglial inclusion filaments in multiple system atrophy. Exp Neurol 2003; 181: 68–78.

Galloway PG, Mulvihill P, Perry G. Filaments of Lewy bodies contain insoluble cytoskeletal elements. Am J Pathol 1992; 140: 809–22.

Gilman S, Low PA, Quinn N, Albanese A, Ben-Shlomo Y, Fowler CJ, et al. Consensus statement on the diagnosis of multiple system atrophy. J Neurol Sci 1999; 163: 94–8.

Gilman S, Wenning GK, Low PA, Brooks DJ, Mathias CJ, Trojanowski JQ, et al. Second consensus statement on the diagnosis of multiple system atrophy. Neurology 2008; 71: 670–6.

Hirohata M, Ono K, Morinaga A, Yamada M. Non-steroidal anti-inflammatory drugs have potent anti-fibrillogenic and fibril-destabilizing effects for alpha-synuclein fibrils in vitro. Neuropharmacology 2008; 54: 620–7.

Inoue M, Yagishita S, Ryo M, Hasegawa K, Amano N, Matsushita M. The distribution and dynamic density of oligodendroglial cytoplasmic inclusions (GCIs) in multiple system atrophy: a correlation between the density of GCIs and the degree of involvement of striatonigral and olivopontocerebellar systems. Acta Neuropathol 1997; 93: 585–91.

Iwata R, Pascali C, Bogni A, Miyake Y, Yanai K, Ido T. A simple loop method for the automated preparation of (11C)raclopride from (11C)methyl triflate. Appl Radiat Isot 2001; 55: 17–22.

Jewett DM. A simple synthesis of [11C]methyl triflate. Int J Rad Appl Instrum [A] 1992; 43: 1383–5.

Johansson A, Savitcheva I, Forsberg A, Engler H, Langstrom B, Nordberg A, et al. [(11)C]-PIB imaging in patients with Parkinson's disease: preliminary results. Parkinsonism Relat Disord 2008; 14: 345–7.

Kudo Y, Okamura N, Furumoto S, Tashiro M, Furukawa K, Maruyama M, et al. 2-(2-[2-Dimethylaminothiazol-5-yl]ethenyl)-6-(2-[fluoro]ethoxy)benzoxazole: a novel PET agent for in vivo detection of dense amyloid plaques in Alzheimer's disease patients. J Nucl Med 2007; 48: 553–61.

Logan J. Graphical analysis of PET data applied to reversible and irreversible tracers. Nucl Med Biol 2000; 27: 661–70.

Maetzler W, Reimold M, Liepelt I, Solbach C, Leyhe T, Schweitzer K, et al. [11C]PIB binding in Parkinson's disease dementia. Neuroimage 2008; 39: 1027–33.

Marti MJ, Tolosa E, Campdelacreu J. Clinical overview of the synucleinopathies. Mov Disord 2003; 18(Suppl): S21–7.

Mathis CA, Wang Y, Holt DP, Huang GF, Debnath ML, Klunk WE. Synthesis and evaluation of 11C-labeled 6-substituted 2-arylbenzothiazoles as amyloid imaging agents. J Med Chem 2003; 46: 2740–54.

Mochizuki A, Mizusawa H, Ohkoshi N, Yoshizawa K, Komatsuzaki Y, Inoue K, et al. Argentophilic intracytoplasmic inclusions in multiple system atrophy. J Neurol 1992; 239: 311–6.

Ono K, Yamada M. Antioxidant compounds have potent anti-fibrillogenic and fibril-destabilizing effects for alpha-synuclein fibrils in vitro. J Neurochem 2006; 97: 105–15.

Ozawa T, Paviour D, Quinn NP, Josephs KA, Sangha H, Kilford L, et al. The spectrum of pathological involvement of the striatonigral and olivopontocerebellar systems in multiple system atrophy: clinicopathological correlations. Brain 2004; 127: 2657–71.

Papp MI, Lantos PL. The distribution of oligodendroglial inclusions in multiple system atrophy and its relevance to clinical symptomatology. Brain 1994; 117(Pt 2): 235–43.

Sakamoto M, Uchihara T, Nakamura A, Mizutani T, Mizusawa H. Progressive accumulation of ubiquitin and disappearance of alpha-synuclein epitope in multiple system atrophy-associated glial cytoplasmic inclusions: triple fluorescence study combined with Gallyas-Braak method. Acta Neuropathol 2005; 110: 417–25.

Shy GM, Drager GA. A neurological syndrome associated with orthostatic hypotension: a clinical-pathologic study. Arch Neurol 1960; 2: 511–27.

Stefanova N, Reindl M, Neumann M, Haass C, Poewe W, Kahle PJ, et al. Oxidative stress in transgenic mice with oligodendroglial alpha-synuclein overexpression replicates the characteristic neuropathology of multiple system atrophy. Am J Pathol 2005; 166: 869–76.

Takahashi H, Wakabayashi K. Controversy: is Parkinson's disease a single disease entity? Yes. Parkinsonism Relat Disord 2005; 11(Suppl 1): S31–7.

Tashiro M, Okamura N, Furumoto S, Kumagai K, Furukawa K, Sugi K, et al. Quantitative analysis of amyloid deposition in Alzheimer's disease patients and healthy volunteers using PET and [11C]BF-227. In: Proceedings of the International Symposium on Early Detection and Rehabilitation Technology of Dementia 2009 (DRD2009). Okayama, Japan, 2009.110–1.

Tong J, Wong H, Guttman M, Ang LC, Forno LS, Shimadzu M, et al. Brain alpha-synuclein accumulation in multiple system atrophy, Parkinson's disease and progressive supranuclear palsy: a comparative investigation. Brain 2010; 133: 172–88.

van der Eecken H, Adams RD, van Bogaert L. Striopallidal-nigral degeneration. An hitherto undescribed lesion in paralysis agitans. J Neuropathol Exp Neurol 1960; 19: 159–61.

Wakabayashi K, Takahashi H. Cellular pathology in multiple system atrophy. Neuropathology 2006; 26: 338–45.

Wakabayashi K, Yoshimoto M, Tsuji S, Takahashi H. Alpha-synuclein immunoreactivity in glial cytoplasmic inclusions in multiple system atrophy. Neurosci Lett 1998; 249: 180–2.

Ye L, Velasco A, Fraser G, Beach TG, Sue L, Osredkar T, et al. In vitro high affinity alpha-synuclein binding sites for the amyloid imaging agent PIB are not matched by binding to Lewy bodies in postmortem human brain. J Neurochem 2008; 105: 1428–37.

Original Paper

Fetal Diagnosis and Therapy

Fetal Diagn Ther 2010;28:79–86
DOI: 10.1159/000316102

Received: October 12, 2009
Accepted after revision: May 25, 2010
Published online: July 31, 2010

Effects of Antenatal Steroid Therapy on Neurodevelopment in an IUGR Mouse Model

Clarissa Velayo[a] Takuya Ito[b] Hiroshi Chisaka[a] Nobuo Yaegashi[a]
Kunihiro Okamura[a] Yoshitaka Kimura[a, b]

[a]Department of Obstetrics and Gynecology, Tohoku University Graduate School of Medicine, and
[b]International Advanced Research and Education Organization, Tohoku University, Sendai, Japan

Key Words
Antenatal steroid therapy · Dexamethasone · Intrauterine growth restriction mouse model · Maternal protein restriction, mice · Postnatal neurodevelopment

Abstract
Background/Objective: To investigate the neurodevelopmental response in postnatal mice secondary to antenatal steroid treatment in association with maternal protein restriction. ***Methods:*** C57BL/6N pregnant mice (n = 24; 4 per treatment group) were administered control (C) or protein-restricted (PR) diets and subjected to daily subcutaneous injection stress during late gestation (E10–E17) with either 100 μl/kg of dexamethasone sodium phosphate in normosaline (C-D/S, PR-D/S) or normosaline alone (C-S, PR-S). Non-treatment groups were also included (C, PR). Brain samples of pups were collected on postnatal day 7 and analyzed by immunohistochemistry and qRT-PCR. ***Results:*** Neonatal weights in the treatment groups were smaller than their counterparts in the C group, but there were no significant differences in brain size. Immunohistochemical evaluation of neuroglial cells revealed a pronounced effect of protein restriction on oligodendrocytes and oligodendrocyte precursor cells with distinct fetal responses to stress and dexamethasone. Further evaluation using quantitative RNA analysis showed significant activation of *Galr1*, *Galr2*, *Igfbp-1*, *Igfbp-3*, *Igfbp-6*, and *Fgf2* by 1- to 2.5-fold in the PR-D/S group and by much higher increments, 1- to 10.5-fold, in the PR-S group. ***Conclusion:*** This preliminary investigation revealed the possible role of dexamethasone in further increasing vulnerability to cell damage in injury-prone neuroglial cells. The distribution of key glial markers and the overexpression of several neurotrophic factors depicted ongoing cellular adaptation.

Introduction

At the present time, antenatal steroid therapy is an option for which the benefits seem to outweigh the risks, but this generalization may not apply to all patients. There are two types of preterm infants according to birth weight: (1) preterm infants with appropriate weight for gestational age, and (2) preterm infants with low birth weight for gestational age. The latter group is known to be more susceptible to chronic diseases and diseases of adult onset [1]. This vulnerability may be attributed to adaptive responses during development secondary to environmental stimuli such as maternal diet modification and stress which instigate changes in fetal programming.

KARGER
Fax +41 61 306 12 34
E-Mail karger@karger.ch
www.karger.com

1015–3837/10/0282–0079$26.00/0

Accessible online at:
www.karger.com/fdt

Clarissa Velayo, MD
Department of Obstetrics and Gynecology
Tohoku University Graduate School of Medicine
1-1, Seiryomachi, Aoba-ku, Sendai 980-8574 (Japan)
Tel. +81 22 717 7251, Fax +81 22 717 7258, E-Mail chinkeyvelayo@yahoo.com

In this study, a novel approach to understanding fetal adaptive response as graded events is presented. All structural levels may be observed to follow a temporal pattern of events wherein acute and chronic responses depend on surpassing specific thresholds. A primary exposure that does not surpass the threshold for an adaptive response results in sensitization with minimal changes to the developing fetus. On the other hand, single or cumulative exposures that surpass the threshold can mount an adaptive response. Furthermore, graded events before and after the attainment of such thresholds have also been observed in this study. A hyperreactive response, occurring in pre-sensitized fetuses, will exhibit lower thresholds while a restrained response is a subdued or muted change observed in pre-sensitized fetuses in the presence of dexamethasone.

This study uses protein restriction in a mouse model for simulation of intrauterine growth restriction (IUGR) and focuses on the effects of antenatal steroid therapy on postnatal neurodevelopment. The neuroplasticity of glial cells allows for the observation of such changes. Through the use of stage-specific markers, different glial populations can be delineated during embryonic brain development [2–4]. For our study purposes, two types of glial cells were evaluated: oligodendrocytes *(Mbp* and *Pdgfrα)* and astrocytes *(Gfap)* – both of which are derived from a common precursor *(Olig2)*.

In addition, specific gene expression was evaluated to characterize ongoing cellular adaptation. Numerous investigations concerning the different oligodendrocyte lineage cells have reported that these genes are regulators of growth *(Igfbp-1, Igfbp-3,* and *Igfbp-6)* and have neuroprotective properties *(Galr1, Galr2,* and *Fgf2)* among which include the prevention of demyelination and the enhancement of neurogenesis after injury [5–13].

Thus, neonatal brain phenotypic attributes neuroglial protein patterns and mRNA expression of neurotrophic genes were evaluated for their response to dexamethasone treatment.

Materials and Methods

Animals

Female C57BL/6N mice (n = 24), about 6 weeks old, provided by the Institute for Animal Experimentation, Tohoku University Graduate School of Medicine, were maintained under controlled lighting (12-hour light cycles) and temperature (24°C). These were allowed free access to food (AIN-93G; Oriental Yeast Co. Ltd, Tokyo, Japan) and water during a 2-week acclimatization period after which each female was time mated with a male.

Treatment Groups

Pregnant females were housed singly and administered either control (C) or protein-restricted (PR) diets (online suppl. table 1, www.karger.com/doi/10.1159/000316102) ad libitum all throughout pregnancy (embryonic stage, E0–E17) and after delivery (postnatal stage, P0–P7). These were further subdivided into six groups (n = 4 per group) where each received a single or combination of treatments during late gestation (E10–E17). More specifically, this consisted of daily subcutaneous injection stress with either plain normosaline solution (C-S, PR-S) or 100 μl/kg dexamethasone sodium phosphate (Decadron®; MSD Banyu Pharmaceutical Co. Ltd, Japan) in normosaline solution (C-D/S, PR-D/S). Non-treatment groups were also included (C, PR). All injections were performed between 12 and 2 p.m. Maternal weights on days E0, E10, and E17 were recorded, as well as neonatal weights on P7.

Whole Brain Sampling

On postnatal day 7, separate brain sampling techniques were performed. For brain size and immunohistochemical analyses (n = 96; 16 per treatment), 2 male and 2 female pups from each litter were anesthetized by isoflurane inhalation (Forane® Isoflurane; Abbott Japan Co. Ltd, Japan) and perfused intracardially with 4% paraformaldehyde. Whole brains were collected and supercooled in dry ice for 30 min before storage at –20°C. These were subsequently mounted using an OCT compound (Tissue-Tek® 4583; Sakura Finetek Japan, Co. Ltd, Tokyo, Japan) and cut on a cryostat (Leica Cryostat CM3050 S; Leica, Wetzlar, Germany) to obtain 14-μm coronal sections at the level of the lateral ventricle (bregma = 0–0.74 mm, interaural = 3.80–4.39 mm). All specimens were collected on APS-coated Superfrost glass microslides (Matsunami Glass Ind. Ltd, Osaka, Japan) and air dried. Sections were stored at –80°C. Meanwhile for RNA analysis, whole brain samples from the remaining pups in each litter (n = 42; 7 per treatment) underwent initial processing for later RNA extraction. The same anesthetic procedure mentioned earlier was applied prior to brain dissection followed by supercooling in liquid nitrogen and storage at –80°C.

Fetal Brain Size Analysis

Slide sections were stained with hematoxylin (Gill's Hematoxylin 2003-2; Muto Pure Chemicals Co. Ltd., Japan) and eosin (Eosin Alcohol Solution acid extract 050-06041; Wako Pure Chemicals, Ind. Ltd, Japan). Images were captured on a Leica CTR 5000 and DM 5000B microscope system (Leica). Using Adobe® Photoshop® CS4 Extended software, specific brain portions were manually traced on each of the captured digital images and the total number of pixels within traced areas was determined. Individual cortical thicknesses as well as corpus callosum indices were analyzed. The latter was equal to the ratio of the area of the corpus callosum and the cortical thickness.

Immunohistochemistry

A total of 16 fetal brains (8 male, 8 female) per treatment group were examined. Sections were blocked with 4% paraformaldehyde for 15 min and incubated with the primary antibody at 4°C overnight. Coupled secondary antibodies were used for single and double labeling. Slides were mounted with Vectashield® medium (Vector Laboratories, Inc., Burlingame, Calif., USA) and coverslipped. The following primary antibodies were used: Mbp (Rat

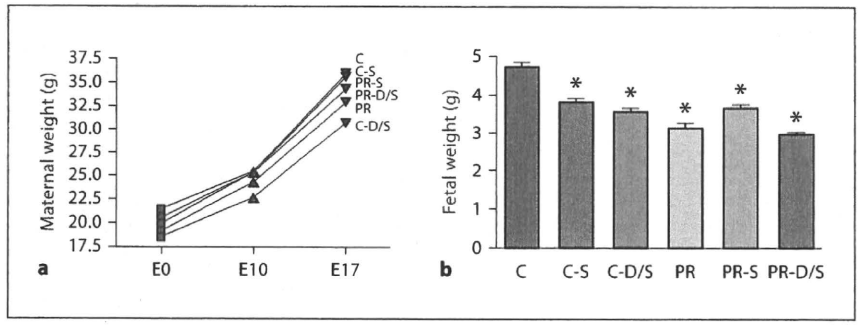

Fig. 1. Effects of treatment on weight gain. **a** Each data point represents maternal weight as mean ± SD (n = 4 per treatment). Two-way ANOVA indicates a significant treatment effect ($p < 0.0001$) and time effect ($p < 0.0001$). Bonferroni post-test indicates that, with the exception of the PR and C-D/S groups at E17, all treatments were similar to the C group. **b** Mean fetal weights across treatments ± SEM were significantly different by one-way ANOVA ($p < 0.0001$; n = 193). Bonferroni post-test indicates significant variation of the C group with all other treatment groups (* $p < 0.001$).

Anti-Myelin basic protein 82–87 region IgG; 1:200; Chemicon International, Inc., Temecula, Calif., USA), Gfap (Rabbit anti-glial fibrillary acidic protein IgG; 1:800; Sigma, St. Louis, Mo., USA), Olig2 (Anti-Human Olig2 Rabbit IgG Affinity Purity; 1:1,000; IBL, Co. Ltd, Japan), and Pdgfrα (Purified rat anti-mouse CD140a (PDGF Receptor α chain monoclonal antibody IgG; 1:500; BD Pharmingen, San Diego, Calif., USA). 4′6-Diamidino-2-phenylindole, dihydrochloride (DAPI) FluoroPure™ grade (1:500; Molecular Probes, Inc., Eugene, Oreg., USA) was used to identify the nuclei. The following secondary antibodies were used: Alexa Fluor® 488 donkey anti-rabbit IgG (1:500; Invitrogen, Eugene, Oreg., USA) and Cy™3-conjugated Affini-Pure Donkey anti-rat IgG (1:500; Jackson ImmunoResearch Laboratories, Inc., West Grove, Pa., USA). Images were captured on a Leica CTR 5000 and DM 5000B microscope system (Leica). Neuroglial protein marker expression was analyzed using Adobe Photoshop® CS4 Extended software. Specific brain portions were manually traced on each of the captured digital images. Protein marker expression was equivalent to the degree of fluorescence observed (pixels of fluorescence/total number of pixels) (online suppl. fig. 1).

Quantitative PCR

Total RNA was extracted from whole fetal brains using QIAzol Lysis Reagent (Qiagen, Hilden, Germany) and cleaned with an miRNeasy kit (Qiagen) according to the manufacturer's protocol. Complementary DNA was synthesized using the Superscript™III First-Strand Synthesis System (Invitrogen, Carlsbad, Calif., USA) and quantitative PCR was conducted with Express SYBR® GreenER™ Supermix with Premixed ROX (Invitrogen) on an Eppendorf *Realplex*^{2} Mastercycler (Eppendorf, Hamburg, Germany). Primer sequences of the resulting significant genes are provided (online suppl. table 2).

Statistical Analysis

One-way analysis of variance (ANOVA) was conducted between treatment groups for each procedure. Post-hoc analysis (Bonferroni post-test) was also used where applicable. All tests were performed using GraphPad Prism® 4 software.

Results

Maternal weight gain patterns between groups were similar before (E0–E10) and during treatment (E10–E17). There were no differences in timing of delivery (E18 or P0), litter size, and litter sex distribution. Mean neonatal weights on postnatal day 7 between treatment groups were significantly different ($p < 0.0001$; n = 193) showing a mean decrease of all groups compared to the C group (fig. 1). However, fetal brain size across treatment groups were similar (n = 91). The cortical thickness between treatment groups did not differ and corpus callosum indices revealed proportionality of this area to cortical thickness independent of the treatment received (fig. 2).

Immunohistochemical Analysis

The immunohistochemical analysis of *Mbp* and *Gfap* expression, mature oligodendrocyte and astrocyte markers, respectively, demonstrated that astrocyte populations were less affected by protein restriction or injection stress. However, like oligodendrocyte populations, these were not resilient against dexamethasone (fig. 3).

Diet-affected patterns across treatment groups in the corpus callosum *(cc)* were notably similar between *Mbp* and *Pdgfrα* (fig. 3, 4) revealing a more pronounced effect on oligodendrocytes. For *Pdgfrα* and *Olig2*, the additional analysis of adjacent brain areas such as the subventricular zone *(svz)* (fig. 4c, f) and caudate putamen *(cpu)* (fig. 4d, g) exhibited the same expression patterns producing no geographical distinction.

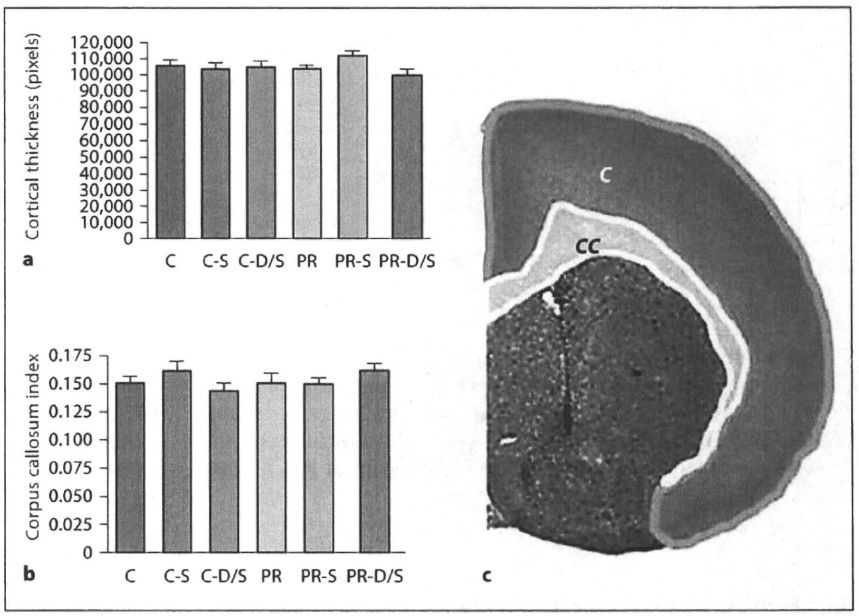

Fig. 2. a, b Cortical thickness and corpus callosum indices suggested similarity between fetal brain size across treatments with standard error bars included (n = 91). **c** The corpus callosum index was equal to the ratio of the area of the corpus callosum *cc* and the cortical thickness *c*.

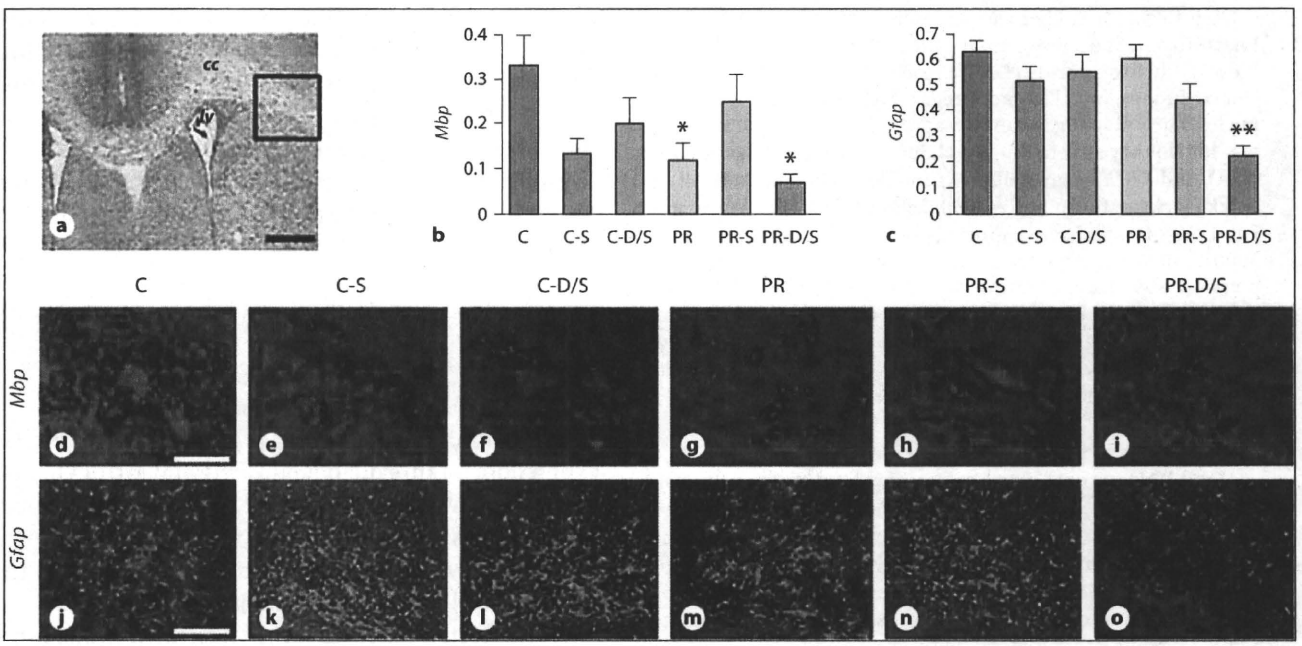

Fig. 3. Mbp and Gfap expression in the six treatment groups. **a** Box inset shows the approximate area measured in the corpus callosum *cc* in a coronal section at the level of the lateral ventricle *lv* using hematoxylin and eosin staining. **b, c** Graphical representations summarizing immunohistochemical results as ratio of positive area by *cc* area for each marker (standard error bars included). One-way ANOVA indicates significant variation in both *Mbp* ($p < 0.0027$; n = 85) and *Gfap* ($p < 0.0001$; n = 86). A comparison to the C group by Bonferroni post-test shows significant variation with the PR (* $p < 0.05$) and PR-D/S (* $p < 0.01$; ** $p < 0.001$) groups. **d–o** Representative images for each treatment group showing *Mbp* (**d–i**) and *Gfap* (**j–o**) expression at a magnification of 20×. Scale bars: **a** = 500 μm, **d–o** = 200 μm.

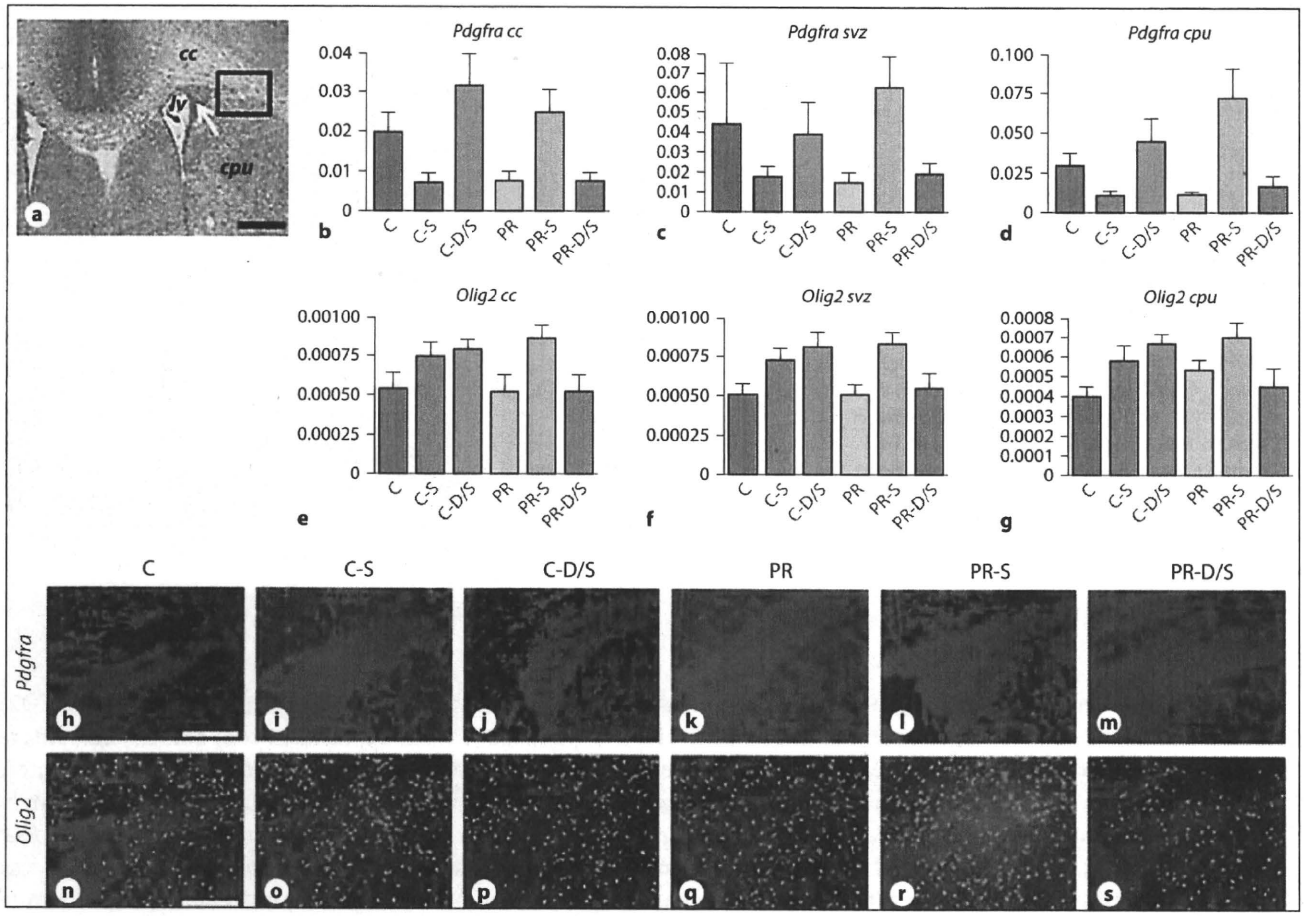

Fig. 4. *Pdgfra* and *Olig2* expression in the six treatment groups. **a** Box inset shows the approximate area measured in a coronal section at the level of the lateral ventricle *(lv)* using HE staining; corpus callosum *(cc)*; caudate putamen *(cpu)*; white arrow, subventricular zone *(svc)*. **b–g** Graphical representations summarizing immunohistochemical results as ratio of positive area by specified brain area for each marker (standard error bars included). Statistical analyses were significant using one-way ANOVA for *Pdgfra cc* ($p < 0.0002$; $n = 85$), *Pdgfra cpu* ($p < 0.0001$; $n = 85$), *Olig2 cc* ($p < 0.0240$; $n = 83$), *Olig2 svz* ($p < 0.0044$; $n = 83$), and *Olig2 cpu* ($p < 0.0166$; $n = 83$). **h–s** Representative images for each treatment group showing *Pdgfra* (**h–m**) and *Olig2* (**n–s**) expression at a magnification of 20×. Scale bars: **a** = 500 μm, **h–s** = 200 μm.

mRNA Analysis

Quantitative RNA analysis showed significant activation ($p < 0.0001$) of *Galr1*, *Galr2*, *Igfbp-1*, *Igfbp-3*, *Igfbp-6*, and *Fgf2* by 1- to 2.5-fold in the PR-D/S group and by much higher increments, 1- to 10.5-fold, in the PR-S group (fig. 5).

Discussion

The expression patterns across treatment groups were indicative of varying responses to injury in both oligodendrocyte and astrocyte lineage cells. First, there were different effects between neuroglial cell types secondary to primary injury. Second, the effect of protein restriction on oligodendrocyte distribution patterns was more pronounced, but the specific precursor cell lineage most affected was not determined, and third, significant genes pointed towards oligodendrocyte susceptibility and myelination effects. From these, a key response to dexamethasone was seen as a recurring pattern in the PR-S and PR-D/S groups in both immunohistochemical evaluation and mRNA analysis (fig. 3–5).

Maintaining glucocorticoid homeostasis necessitates a delicate balance between maternal and fetal environments. Our results suggested that mice in the C diet treat-

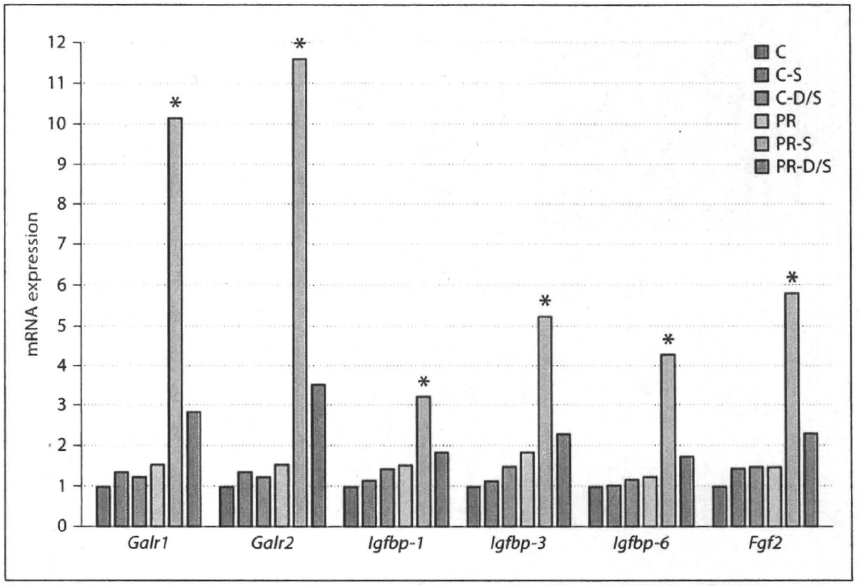

Fig. 5. Quantitative mRNA analysis. There was significant activation by one-way ANOVA ($p < 0.0001$; $n = 24$ per gene) of *Galr1, Galr2, lgfbp-1, Igfbp-3, lgfbp-6,* and *Fgf2* by 1- to 2.5-fold in the PR-D/S group and by much higher increments, 1- to 10.5-fold, in the PR-S group. Bonferroni post-test indicated * $p < 0.001$ for PR-S. Individual gene graphs with standard error reports were submitted as online supplementary figure 1.

ment groups were able to maintain varying levels of glucocorticoid homeostasis amidst chronic stress (daily subcutaneous injections from E10 to E17) or the presence of dexamethasone. In C group offspring, exposure to normal levels of maternal cortisol was successfully blocked. In C-S offspring, increased levels of maternal endogenous cortisol overwhelmed this natural protective barrier and led to significant fetal exposure. Both exogenous and eventually endogenous corticosteroids resulted in IUGR effects at phenotypic and molecular levels. C-S fetuses were sensitized or became susceptible to any further change. In the C-D/S offspring, IUGR was evident, but the addition of dexamethasone resulted in an adaptive fetal response not observed with stress alone. In terms of neurodevelopmental effects, our results showed that this was a beneficial or protective response to stress.

On the other hand, mice in the PR diet groups were basically at a disadvantage prior to stress or dexamethasone treatment. The offspring of PR groups were pre-sensitized. Aside from exhibiting IUGR, they most likely had dysfunctional placentas. With the addition of chronic stress (PR-S), a protective hyperreactive fetal response was observed, but this response was markedly restrained in the presence of dexamethasone (PR-D/S). The latter suggested detrimental effects to neurodevelopment in the last treatment group.

The presence of a protective barrier system between this interplay of maternal and fetal environments is crucial. Current investigations have focused on the role of 11β-hydroxysteroid dehydrogenase type 2 (11-βHSD2) as a possible placental glucocorticoid barrier, and interestingly, 11-βHSD2 activity is decreased during maternal protein restriction or stress [14]. This would explain how high maternal cortisol concentrations were able to saturate the limited enzyme available allowing any excess to pass through unchanged. This presents distinct similarities with our study conditions, but the presence of 11-βHSD2 alone cannot account for the graded fetal response observed or the isolated effects of dexamethasone.

Dexamethasone was administered subcutaneously thereby effectively bypassing maternal liver metabolism. It was also less difficult for this glucocorticoid to reach the fetus because it has been known to be a poor substrate for placental 11-βHSD2 [15]. Two possible explanations for the observed isolated dexamethasone effects in contrast to cortisol were as follows: first, the supraphysiological levels and potency of dexamethasone may have produced these damaging effects. Dexamethasone was notably the more potent glucocorticoid with a potency range of 25–80 and $t_{1/2}$ (half-life in hours) of 36–54, as compared to cortisol with a potency of 1 and $t_{1/2}$ of 8 [16]. Second, due to anti-inflammatory properties which have not been fully elucidated yet, corticosteroids bind to receptors and form complexes that target genes in the nucleus [17]. It is possible that there was differential regulation of target genes between dexamethasone and cortisol, or due to individual properties, they differed entirely in terms of specific genes targeted. Furthermore, suppression of the

fetal HPA axis could not possibly account for all phenotypic results and underlying genotypic alterations. More likely, the effects of dexamethasone result from a collective response from various structural levels (molecular to cellular) both involving fetal neurometabolic factors and maternal adaptation to pregnancy.

Our IUGR mouse model developed at the Tohoku University has been modified for different investigative projects [18–22], but its main premise asserts that maternal malnutrition in mice affects offspring and acts as a primary insult or an acquired susceptibility resulting in phenotypic and genotypic changes. In addition, this study also recognized another primary insult as stress in the form of an injection. This implication is supported by various studies where injection of a vehicle alone was not equivalent to a placebo due to resulting behavioral and biochemical modulation [23, 24]. In the analysis of this study, understanding these two sources of primary insults and their roles in each treatment group helped to delineate which effects of those observed were truly attributable to dexamethasone alone. The treatment groups where only a primary injury was involved (C-S, PR) may or may not have shown marked differences from the C group, but their underlying sensitization to further injury can be inferred from the behavior of double injury treatments (C-D/S, PR-S).

Another concern was the brain area chosen in the experiment. Conventional reports focus on the hippocampus, but more investigations have started to look at other subcortical areas, such as the corpus callosum and subventricular zone, where there also exists high neuroplastic potential extending into the postnatal and adult period [4–6]. Moreover, oligodendrocyte lineage precursors have been demonstrated to migrate from different parts of the telencephalic ventricular zone towards various neural segments in waves beginning in the late gestation [4]. Thus, an examination of glial movement patterns should be included in future studies.

Dexamethasone: Good or Bad for the Brain?

In summary, prenatal programming, secondary to maternal protein restriction, renders an inherent susceptibility to neural compromise in offspring. This was evident in our study of two neuroglial cell lines. This early vulnerability or pre-sensitization uniquely changes fetal response to further injury as compared to other forms of stress. With the addition of dexamethasone in PR offspring, the restrained response may be seen as more detrimental than beneficial.

Clinical Correlation

Consensus dictates that the benefits should always outweigh the risks. In relation to antenatal steroid therapy, benefits related to organ maturation still mark heavily. Furthermore, the amount of dexamethasone administered to mice in this experiment were at supraphysiological levels and cannot be compared to current practice guidelines on antenatal steroid therapy, but our concern remains for incidences where multiple treatment is necessary in low-birth-weight or IUGR babies. It is for these extreme, but no less important, cases that more studies should attempt to understand beyond the general perception to achieve truly individualized medicine.

Acknowledgements

The authors would like to thank K. Mitsuya, N. Nakamura, J. Sharif, N. Matsuda, and M. Wong-Radescu for their assistance. Dr. Velayo is a Takeda Science Foundation Fellow.

References

1 Seckl JR, Holmes MC: Mechanisms of disease: glucocorticoids, their placental metabolism and fetal 'programming' of adult pathophysiology. Nat Clin Pract Endocrinol Metab 2007;3:479–488.

2 Liu Y, Wu Y, Lee JC, Xue H, Pevny LH, Kaprielian Z, et al: Oligodendrocyte and astrocyte development in rodents: an in situ and immunohistological analysis during embryonic development. Glia 2002;40:25–43.

3 Cai J, Chen Y, Cai WH, Hurlock EC, Wu H, Kernie SG, et al: A crucial role for Olig2 in white matter astrocyte development. Development 2007;134:1887–1899.

4 Kessaris N, Fogarty M, Iannarelli P, Grist M, Wegner M, Richardson WD: Competing waves of oligodendrocytes in the forebrain and postnatal elimination of an embryonic lineage. Nat Neurosci 2006;9:173–179.

5 Shen PJ, Larm JA, Gundlach AL: Expression and plasticity of galanin systems in cortical neurons, oligodendrocyte progenitors and proliferative zones in normal brain and after spreading depression. Eur J Neurosci 2003; 18:1362–1376.

6 Shen PJ, Yuan CG, Ma J, Cheng S, Yao M, Turnley AM, et al: Galanin in neuro(glio)-genesis: expression of galanin and receptors by progenitor cells in vivo and in vitro and effects of galanin on neurosphere proliferation. Neuropeptides 2005;39:201–205.

7 Lündstrom L, Elmquist A, Bartfai T, Langel Ü: Galanin and its receptors in neurological disorders. Neuromol Med 2005;7:157–180.

8 Hobson SA, Bacon A, Elliot-Hunt CR, Holmes FE, Kerr NCH, Pope R, et al: Galanin acts as a trophic factor to the central and peripheral nervous systems. Cell Mol Life Sci 2008;65:1806–1812.

9 Zumkeller W: The effect of insulin-like growth factors on brain myelination and their potential therapeutic application in myelination disorders. Eur J Paediatr Neurol 1997;4:91–101.
10 Kühl NM, Hoekstra D, De Vries H, De Keyser J: Insulin-like growth factor-binding protein 6 inhibits survival and differentiation of rat oligodendrocyte precursor cells. Glia 2003;44:91–101.
11 Jin K, LaFevre-Bernt M, Sun Y, Chen S, Gafni J, Crippen D, et al: FGF-2 promotes neurogenesis and neuroprotection and prolongs survival in a transgenic mouse model of Huntington's disease. Proc Natl Acad Sci USA 2005;102:18189–18194.
12 Molteni R, Fumagalli F, Magnaghi V, Roceri M, Gennarelli M, Racagni G, et al: Modulation of fibroblast growth factor-2 by stress and corticosteroids: from development events to adult brain plasticity. Brain Res Rev 2001;37:249–258.
13 Bansal R, Magge S, Winkler S: Specific inhibitor of FGF receptor signaling: FGF-2-mediated effects on proliferation, differentiation, and MAPK activation are inhibited by PD173074 in oligodendrocyte-lineage cells. J Neurosci Res 2003;74:486–493.
14 Drake AJ, Walker BR, Seckl JR: Intergenerational consequences of fetal programming by in utero exposure to glucocorticoids in rats. Am J Physiol 2005;288:R34–R38.
15 Seckl JR, Cleasby M, Nyirenda MJ: Glucocorticoids, 11β-hydroxysteroid dehydrogenase, and fetal programming. Kidney Int 2000;57:1412–1417.
16 Felig P, Frohman LA: Endocrinology and Metabolism. New York, McGraw-Hill, 2001.
17 Doan T, Melvold R, Viselli S, Waltenbaugh C: Lippincott's Illustrated Reviews: Immunology. Philadelphia, Lippincott Williams & Wilkins, 1997.
18 Neugebauer R, Hoek HW, Susser E: Prenatal exposure to wartime famine and development of antisocial personality disorder in early adulthood. JAMA 1999;281:455–462.
19 Baum DA, Smith SD, Donovan SS: The tree-thinking challenge. Science 2005;310:979–980.
20 Sharif J, Nakamura M, Ito T, Kimura Y, Nagamune T, Mitsuya K, et al: Food restriction in pregnant mice can induce changes in histone modifications and suppress gene expression in fetus. Nucleic acids Symp Ser (Oxf) 2007;51:125–126.
21 Matsuda N, Velayo C, Ito T, Chisaka H, Yaegashi N, Kimura Y, Okamura K, Sharif J: Gestational stage- and sex-specific impact of maternal folate deficiency on fetal growth and epigenetic regulation of gene expression in the fetus. Reprod Sci Suppl 2009;16:140A–141A.
22 Velayo C, Matsuda N, Ito T, Chisaka H, Yaegashi N, Kimura Y, Okamura K, Sharif J: Maternal protein restriction during late gestation induces sex-specific and reciprocal regulation of the Igf2/Igfbp1 gene expression ratio in placenta: a possible association between nutrition and epigenetics. Reprod Sci Suppl 2009;16:347A–347A.
23 Meijer MK, Spruijt BM, van Zutphen LFM, Baumans V: Effect of restraint and injection methods on heart rate and body temperature in mice. Lab Anim 2006;40:382–391.
24 Ryabinin AE, Wang YM, Finn DA: Different levels of Fos immunoreactivity after repeated handling and injection stress in two inbred strains of mice. Pharm Biochem Behav 1999;63:143–151.

Development, Growth & Differentiation

The Japanese Society of Developmental Biologists

Develop. Growth Differ. (2011) **53**, 357–365

doi: 10.1111/j.1440-169X.2010.01235.x

Original Article

Differentiation of neuronal cells from NIH/3T3 fibroblasts under defined conditions

Zhuo Wang, Eriko Sugano, Hitomi Isago, Teru Hiroi, Makoto Tamai and Hiroshi Tomita*

Tohoku University Institute for International Advanced Interdisciplinary Research, 4-1 Seiryo-machi, Aoba-ku, Sendai 980-8575, Japan

We attempted to test whether the differentiated NIH/3T3 fibroblasts could be differentiated into neuronal cells without any epigenetic modification. First, a neurosphere assay was carried out, and we successfully generated neurosphere-like cells by floating cultures of NIH/3T3 fibroblasts in neural stem cell medium. These spheres have the ability to form sub-spheres after three passages, and express the neural progenitor markers Nestin, Sox2, Pax6, and Musashi-1. Second, after shifting to a differentiating medium and culturing for an additional 8 days, cells in these spheres expressed the neuronal markers β-tubulin and neurofilament 200 and the astrocytic marker glial fibrillary acidic protein (GFAP). Finally, after treating the spheres with all-trans retinoic acid and taurine, the expression of β-tubulin was increased and the staining of photoreceptor markers rhodopsin and recoverin was observed. The present study shows that NIH/3T3 fibroblasts can generate neurosphere-like, neuron-like, and even photoreceptor-like cells under defined conditions, suggesting that the differentiated non-neuronal cells NIH/3T3 fibroblasts, but not pluripotent cells such as embryonic stem cells or induced pluripotent stem cells, may have the potential to be transdifferentiated into neuronal cells without adding any epigenetic modifier. This transdifferentiation may be due to the possible neural progenitor potential of NIH/3T3 fibroblasts that remains dormant under normal conditions.

Key words: differentiation, neural progenitors, neuron, retinoic acid, taurine.

Introduction

Because of their ability to proliferate infinitely and differentiate into cells of all three germ layers, embryonic stem (ES) cells are regarded as superior potential donor cells for cell replacement to treat many diseases (Hoffman & Carpenter 2005; Takahashi & Yamanaka 2006), such as retinitis pigmentosa and age-related macular degeneration, which are typically characterized by the death of photoreceptors (Osakada *et al.* 2008). Photoreceptor replacement in the form of a cell-based therapeutic approach may aid in the restoration of vision.

Zhao *et al.* (2002) demonstrated that ES cell-derived neural progenitors expressed regulatory factors needed for retinal differentiation, and that a small subset of these cells differentiated along the photoreceptor lineage in response to retina-specific epigenetic cues. Ikeda *et al.* (2005) and Osakada *et al.* (2008) generated putative photoreceptors and RPE cells from rodent and primate ES cells by induction with defined factors.

However, in clinical application, the use of ES cells involves ethical problems and immune rejection. Jin *et al.* (2009) demonstrated partial mesenchymal stem cells obtained from umbilical cord blood were able to be differentiated into neuron-like cells or rhodopsin-positive cells *in vitro*. Recently, retinal cells have been generated from mouse- and human-induced pluripotent stem (iPS) cells by introducing four specific factors Oct3/4, Sox2, Klf4, and c-Myc (Takahashi & Yamanaka 2006; Hirami *et al.* 2009; Osakada *et al.* 2009).

Even though the generation and application of iPS cells made it possible to treat patients with their own cell-derived retinal cells, which may resolve the problem of immune rejection, some questions still remain. For example, the introduction of viral vectors and oncogenes c-Myc and Klf4 into the somatic genome limits the utility of iPS cells for patient-specific therapy

*Author to whom all correspondence should be addressed.
Email: hiroshi-tomita@iiare.tohoku.ac.jp
Received 28 June 2010; revised 30 November 2010; accepted 30 November 2010.

(Yamanaka 2007, 2009; Zhou *et al.* 2009). Furthermore, the generation of an iPS cell line takes considerable time (approximately 6 months) and is labor intensive so it can not be generated rapidly (Holden & Vogel 2008).

In the previous studies, most investigators have used undifferentiated cells, such as ES cells, ES cell-derived neural progenitors, bone marrow stromal cells, or iPS cells, as the cell source (Sanchez-Ramos *et al.* 2000; Woodbury *et al.* 2000; Zhao *et al.* 2002; Ikeda *et al.* 2005; Klassen & Reubinoff 2008; Osakada *et al.* 2008; Jin *et al.* 2009). Zhang *et al.* (2010) showed that NIH/3T3 fibroblasts, which are already committed to a specific differentiation destiny, were able to be induced to express neuronal markers, but these cells have to be reprogrammed by adding epigenetic modifiers to make epigenetic modification.

NIH/3T3 fibroblasts, derived from an embryo of the NIH/Swiss mouse, are generally adherently cultured in Dulbecco's modified Eagle's medium (DMEM) supplemented with 10% bovine calf serum, which is the normal culture condition for most investigators. In the present study, we cultured NIH/3T3 cells in a completely different microenvironment to establish whether this cell line could be induced into neuronal cells without adding any epigenetic modifier and to be further induced into retinal photoreceptor-like cells simply by adding taurine and retinoic acid (RA), and we also characterized the mechanism involved.

Materials and methods

Culture of NIH/3T3 fibroblasts

NIH/3T3 fibroblasts were kindly provided by the Cell Resource Center for Biomedical Research, Tohoku University, Japan as a frozen stock. Cells were adherently cultured in DMEM with 10% newborn calf serum (NCS), 1× GlutaMax, and 1× Antibiotic-Antimycotic (Invitrogen/Gibco) on normal tissue culture dishes (uncoated) at 37°C, 5% CO_2, which is referred to as normal conditions (NC).

Generation of neurosphere-like cells (Neurosphere assay)

Neurosphere assays were carried out according to previous studies (Das *et al.* 2006; Brewer & Torricelli 2007) with minimal modifications. Briefly, NIH/3T3 fibroblasts were cultured in suspension in NC or neural stem cell medium (NSCm) on 2.0% agarose-coated dishes at a density of 1×10^5 cells/mL for 5–7 days to detect the ability of these cells to form spheres. NSCm was serum-free and composed of DMEM/F-12, 1× GlutaMax, 1× Antibiotic-Antimycotic, 1× B27 supplement (without vitamin A: Cat. No. 12587), 1× N2 supplement, 20 ng/mL bFGF (basic fibroblast growth factor), and 20 ng/mL EGF (epidermal growth factor). All reagents were obtained from Invitrogen/Gibco. Adherent NIH/3T3 fibroblasts cultured in NC on normal tissue culture dishes were used as a control.

Passage of neurosphere-like cells

After 5–7 days of cultivation, spheres were trypsinized into single cells and resuspended in NSCm. The suspension was plated onto a new 2.0% agarose-coated dish and cultured for another 5–7 days to test the ability of these cells to form secondary spheres.

To examine the proliferative ability and expression of neural progenitor markers of NIH/3T3-derived spheres, after 7 days of floating cultivation for the second passage, the spheres were exposed to 10 μmol/L BrdU (Sigma) to tag the dividing cells and plated onto poly-D-lysine-coated 8-well culture slides (BD Biosciences) for the final 48 h (Das *et al.* 2006). Immunocytochemistry was carried out for double staining analysis of the neural progenitor markers Nestin, Sox2, Pax6, Musashi-1 (Msi1), and BrdU. RNA was isolated from NIH/3T3 cells cultured in different conditions, and real-time polymerase chain reaction (PCR) were performed to compare the expression of neural progenitor markers Nestin and Sox2.

Differentiation of neuron- and glia-like cells

For the differentiating culture, NSCm-cultured spheres were trypsinized into single cells and resuspended in differentiating medium (DM), then plated onto poly-D-lysine-coated 8-well culture slides and cultured for an additional 8 days. In DM, EGF and B-27 supplement (without RA Cat. No.12587) were replaced by 1% serum and standard B-27 supplement (including retinyl acetate: Cat. No. 17504). In addition, brain-derived neurotrophic factor (BDNF: 10 ng/mL) was added to promote the differentiation into neuronal cells, and ciliary neurotrophic factor (CNTF: 20 ng/mL) was added for glial cell differentiation (Yang *et al.* 2005; Das *et al.* 2006; Chen *et al.* 2007; Chojnacki & Weiss 2008; Matsuda *et al.* 2009). Immunocytochemistry was carried out to stain the markers of neurons (β-tubulin and neurofilament 200 [NF200]), astrocytes (glial fibrillary acidic protein [GFAP]), and oligodendrocytes (O4).

Induction of retinal photoreceptor-like cells

For the induction of retinal photoreceptor-like cells, NIH/3T3-derived neuron-like cells were trypsinized and